Appl. Phys. A (2015) 118:1479–1487
DOI 10.1007/s00339-014-8912-3

Applied Physics A
Materials Science & Processing

Collision-induced dissociation of $Nb_xO_y^+$ ($x = 1, 2, y = 2–12$) clusters: crossed molecular beams and collision cell studies

Claudia Mihesan · Pavle Glodić · Michalis Velegrakis

Received: 31 July 2014 / Accepted: 25 November 2014 / Published online: 9 December 2014

Abstract Oxygen-rich niobium oxide clusters are formed by mixing laser-produced Nb plasma with pure oxygen, and their stability is investigated by mass spectrometry and collision-induced dissociation. We use an experimental configuration recently developed by our group, where the cluster ions beam is crossed with a secondary beam of noble gas atoms, and the fragments are rejected by a retarding field energy analyzer. In this way, the relative collision cross sections of $Nb_xO_y^+$ ($x = 1,\ 2,\ y = 2–12$) clusters have been measured and information about their fragmentation channels has been obtained.

1 Introduction

Niobium oxides demonstrate outstanding catalytic properties and have applications in various fields, such as petrochemical industry, catalysis for selective hydrocarbon oxidation, or NO_x conversion for pollution control [1–3]. These applications triggered a series of studies on the preparation, molecular structure–reactivity relation, and their catalytic behavior [4–8].

The catalytic activity of niobium oxide surfaces is not well understood, due to the surface's complexity and inhomogeneity. As an approach to overcoming this difficulty, studies on gas phase molecular ions and ionic clusters can provide insights in the physical and chemical properties of the surface. A few investigations started with studies on gas phase reactions of some small niobium oxide anions [9] and cations [10] and continued with niobium oxide clusters [11–13].

In order to understand their chemical reactivity, the knowledge of the structure and stability of the clusters is crucial. To this end, Castleman et al. [13] have studied the properties of cationic niobium oxide clusters. Based on their experiments on collision-induced dissociation (CID), they found the building blocks and the corresponding cluster stoichiometry of the most stable species. Motivated by the results from these CID experiments, Sambrano et al. [14] have presented a DFT study for neutral Nb_xO_y and cationic $Nb_xO_y^+$ clusters, providing a complementary theoretical study of geometric, thermodynamic, and electronic properties. Furthermore, sophisticated studies on cluster structures have also been done using infrared multiple photon dissociation (IR-MPD) [15] and UV–Vis photofragmentation [16].

In our laboratory, we have used photofragmentation spectroscopy and CID of mass-selected ions to study the stability and the structure of metal-doped noble gas clusters [17] and metal oxide clusters [18–21]. In a similar manner, in this contribution we study the positively charged Nb oxide clusters by time-of-flight mass spectrometry and collisions with noble gas atoms. We measure the clusters' fragmentation cross section using our recent approach

C. Mihesan · P. Glodić · M. Velegrakis (✉)
Institute of Electronic Structure and Laser, Foundation for Research and Technology−Hellas, 700 13 Heraklion, Crete, Greece
e-mail: vele@iesl.forth.gr

C. Mihesan
Centre of Advanced Research in Nanobioconjugates and Biopolymers, "Petru Poni" Institute of Macromolecular Chemistry, 700487 Iasi, Romania

P. Glodić
Department of Chemistry, University of Crete, 71003 Heraklion, Greece

P. Glodić
Vinča Institute of Nuclear Sciences, P.O. Box 522, Belgrade 11001, Republic of Serbia

based on crossed molecular beams [21] compared with the standard CID technique [13, 20, 22–24] The new experimental configuration, which uses a secondary molecular Ne beam crossing perpendicularly the primary cluster beam, and a retarding field energy analyzer (RFEA), is significantly faster and more efficient for obtaining fragmentation cross sections, without mass selection of the individual clusters. Furthermore, information on additional reaction channels (besides fragmentation) activated by cluster ion—atom energetic collisions (such as multi-ionization or Coulomb explosion) can be obtained.

2 Experimental apparatus and methods

2.1 Setup

The differentially pumped molecular beam apparatus used in these experiments has been described in detail previously [21, 25–28]. A molecular beam of niobium oxide clusters is generated in a source chamber by combining the laser ablation of a niobium target with a supersonic expansion of oxygen. The niobium oxide cluster cations are carried and cooled down in the supersonic expansion and subsequently pass through a 4-mm-diameter skimmer into a double-field time-of-flight (TOF) mass spectrometer that can be used either in linear configuration or as a reflectron assembly .

A fast-switching circuit provides a high-voltage pulse V_{acc} (typically 1,500 V), that starts the acceleration of cationic complexes existing in the cluster beam and constitutes the time origin for the time-of-flight spectrum. The accelerated cluster ions possess laboratory-frame kinetic energy $E_{Lab} = q \cdot e \cdot V_{acc}$ eV (e is the electron charge and q the charge state of a given ion). Traversing a field-free region, the ions are separated and detected at different times, according to their mass/charge (m/q) ratio, either directly in a linear arrangement or after reflection from the reflectron assembly. The mass spectrometer is equipped with microchannel plate (MCP) detectors, and the TOF spectra are acquired with a 150-MHz computer-controlled digital oscilloscope. The TOF spectrum is obtained by averaging over 100–200 laser shots and is transferred from the digital scope to the computer and further processed using software developed in our laboratory.

2.2 Fragmentation cross section

The stability and the dynamics properties of the produced clusters have been investigated in detail using collision-induced fragmentation. Collisions between cluster ions AB^+ and neutral noble gas atoms X (Kr or Ne) can result in different reactions (i–v):

$$
\begin{aligned}
AB^+ + X &\rightarrow AB^{+(*)} + X^{(*)} && \text{(i) elastic and/or inelastic scattering}\\
&\rightarrow A^+ + B + X \text{ or } A + B^+ + X && \text{(ii) fragmentation}\\
&\rightarrow AB + X^+ && \text{(iii) charge transfer}\\
&\rightarrow AB^{z+} + X + ze^- && \text{(iv) multi - ionization}\\
&\quad\rightarrow (AB^{z+})^* \rightarrow A^+ + B^{+(z-1)} && \text{(v) Coulomb explosion}
\end{aligned}
$$

With the exception of elastic or inelastic scattering in all the other reaction channels, the ratio m/q of the initial cluster decreases, either by reducing m or by increasing q [21].

When a parent ion with mass m_P having initial kinetic energy E_{Lab} in the laboratory frame dissociates into a fragment with mass m_F, then—neglecting the center of mass kinetic energy release—the laboratory kinetic energy of the fragment m_F is as follows:

$$E_F = (E_{Lab})(m_F/m_P). \quad (1)$$

This relation allows the use of devices sensitive to the kinetic energy of the incident ions to separate fragments from the parents. Such devices are the reflectron and the retarding field energy analyzer, both used in our laboratory for CID experiments in two different arrangements: beam-gas cell and crossed molecular beams (see below and in Ref. [21]).

In both cases, the parent cluster's abundance before and after the interaction (over the distance L) with the collision partner (of number density N) can be described by Beer's law:

$$I = I_0 \exp(-QNL), \quad (2)$$

where I is the (remaining) intensity of nonfragmented clusters, I_0 is their initial intensity, and Q is the fragmentation cross section. By measuring I and I_0 and considering that N and L are the same for all clusters, the relative fragmentation cross section for the cluster series can be determined.

In the conventional experimental arrangement for CID studies, a beam of mass-selected cluster ions passes through a 27-cm-long collision chamber filled with Kr gas at a pressure of 6×10^{-4} mbar. The mass-selected parent cluster and its fragments are recorded as different peaks in the same TOF spectrum, using a reflectron setup [29], and from their intensities, the fragmentation cross section Q can be determined [20, 21].

The second experimental configuration is based on crossed molecular beams and has been described in Ref. [19]. The cluster beam containing the entire distribution of cluster cations crosses, in the field-free zone of the mass spectrometer, a pulsed secondary beam of Ne atoms with pulse duration of 700 μs. Crossed beam experiments can be performed only by proper temporal overlapping of the two beams (configuration noted "beam on"). By introducing a 1-ms time delay, the beam crossing is avoided ("beam off"), while the background pressure is unchanged. This allows the discrimination of fragmentation processes arising from the beam interaction from those due to the background or parent ion metastability. The fragmentation products have almost the same velocity as the parent, and they are detected as part of the same time-of-flight peak but possess lower kinetic energy [Eq. (1)] and therefore can be rejected by the RFEA situated in front of the MCP detector placed in linear configuration in the TOF spectrometer, reducing the intensity of the peak. The RFEA has an energy resolution of about 5 %.

Entire mass spectra are recorded at varying voltages applied on the RFEA grid (V_{grid}), in the range from 0 V to a value significantly higher than the accelerating voltage.

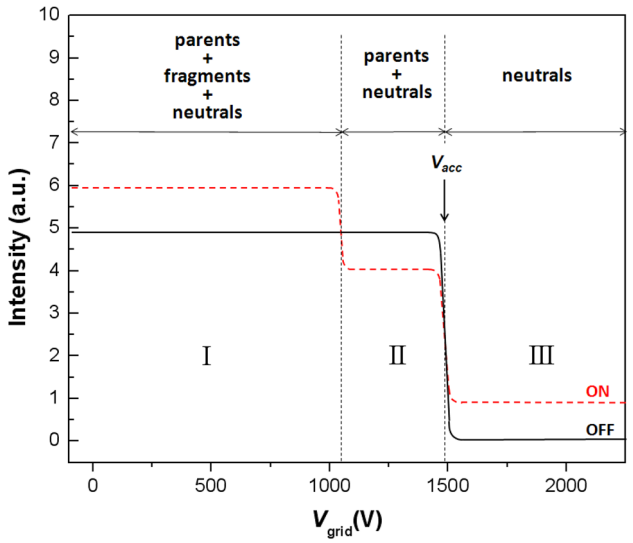

Fig. 1 Intensity dependence on the retarding grid potential for a parent cluster ion undergoing fragmentation with only one ionic fragment. *Solid* and *dashed lines* refer to secondary beam "off" and "on," respectively

From such spectra, the intensity of each cluster can be measured, and Fig. 1 displays the expected evolution of one particular cluster's intensity as a function of RFEA potential, in the simplest case of an ion having only one fragmentation channel ($AB^+ \rightarrow A^+ + B$). The solid line shows the intensity in the "beam off" configuration, and the dashed line displays the intensity expected in "beam on" configuration.

The step-like decrease in the signal at a certain value of V_{grid} indicates the rejection of ions with kinetic energy $E < q{\cdot}e{\cdot}V_{grid}$. As the laboratory velocity of the fragments is not expected to vary significantly, and considering all ions singly charged, their molecular masses can be determined from Eq. (1), hence identifying the fragmentation products.

At low values of the RFEA voltage ($V_{grid} \approx 0$), initially formed clusters and newly formed fragments (ions and neutrals) will have the same time-of-flight and contribute to the same peak, whose intensity represents the total signal [21] (Region I in Fig. 1). Like the ions, fast neutrals impacting a MCP detector produce secondary electrons which result in a measurable signal. In this process, the absolute detection efficiency for both ions and neutrals is similar [30]. The neutrals' energy is given by the initial acceleration voltage, and it is not changed under the influence of the RFEA; therefore, the neutrals' contribution to the total MCP signal is constant and independent of the RFEA voltage. The signal is higher in "beam on" configuration than for "beam off" for every cluster. The difference between the two signals corresponds to fragments (supplementary ions or neutrals formed from the parents). At a RFEA voltage higher than the ionic fragments' kinetic energy but slightly lower than the acceleration voltage ($E_F < V_{grid} \lesssim V_{acc}$), all fragment ions are rejected and the measured intensity includes contributions from nonfragmented parents plus neutrals (Region II). Finally, at V_{grid} significantly higher than the accelerating voltage ($V_{grid} \gg V_{acc}$) all charged species are rejected and only neutral species can reach the detector (Region III).

Referring to Fig. 1 and Eq. (2), the fragmentation cross section for each particular cluster can be obtained by simply recording TOF spectra corresponding to regions II and III in Fig. 1 and measuring the intensity of each cluster. The fragmentation cross section is given by Eq. (3):

$$Q = -\frac{1}{NL}\ln\left(\frac{I_{II}^{ON} - I_{III}^{ON}}{I_{II}^{OFF} - I_{III}^{OFF}}\right), \tag{3}$$

where I_{II}^{ON} and I_{III}^{ON} are signal intensities in "beam on" configuration in region II and III and I_{II}^{OFF} and I_{III}^{OFF} are "beam off" signal intensities in region II and III, respectively (see Fig. 1).

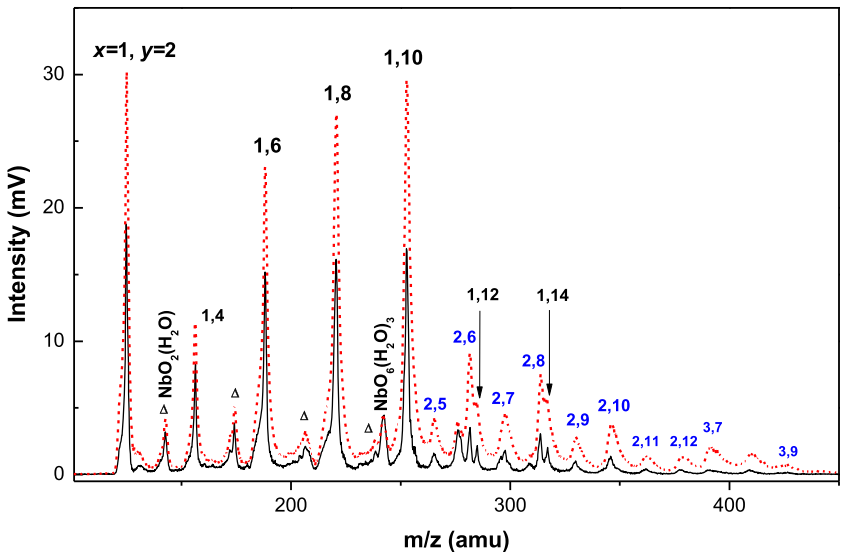

Fig. 2 Mass spectra of niobium oxide clusters $Nb_xO_y^+$ obtained at $V_{grid} \approx 0$, with beam crossing (*dashed line*) and without beam crossing (*solid line*). The *open triangle* indicates the hydrated clusters (see text for details)

3 Results and discussion

3.1 Mass spectra

In Fig. 2, we present mass spectra of the cationic niobium oxide clusters formed in our source, obtained in linear TOF configuration, with and without the secondary beam crossing (dashed and full line, respectively). The $Nb_xO_y^+$ cluster ions peaks are labeled as *x,y*, ranging from 1,2 to 3,7. The O content of the clusters does not affect much the ionization potential of Nb_mO_n clusters, [31] so the mass spectrum recorded in "beam off" configuration represents the initial distribution of cluster ions produced directly from the plasma/oxygen mixing.

The main species are a series of NbO_y^+ ($y \leq 14$) cluster ions, starting at NbO_2^+. Contrary to experiments using a pure He beam as carrier gas, [32] by adding O_2, [13, 33] or using pure O_2 as carrier gas in our case, no atomic ion (Nb^+) or niobium monoxide (NbO^+) are detected, due to their exothermic reactions with oxygen. [34, 35] The dominant production of cluster ions containing one metal atom is observed and discussed in several previous studies [18, 36] performed by our group. The configuration of our cluster source—without confining channels—limits the number of metal–metal collisions, necessary for the formation of clusters containing more than one metal atom. Nevertheless, small amounts of $Nb_2O_y^+$ ($y = 2$–15) and $Nb_3O_{7-9}^+$ were also detected.

The NbO_y^+ series consists mostly of clusters with an even number of oxygen atoms. The absence of clusters with an odd number of O atoms differs from earlier studies [13, 15, 37], where both even- and odd-numbered clusters were formed. A similar odd–even alternation is noticed for $Nb_2O_y^+$ cluster series, but not as prominent as in the case of NbO_y^+ clusters. The use of pure O_2 reacting with the Nb ablation plume leads to the formation of clusters very rich in oxygen. [38–40] Although not so strong, this effect is also seen in the distribution of $Nb_2O_y^+$ clusters, where $Nb_2O_6^+$ cluster is the most intense of the series. Additionally, hydrated clusters (marked by triangles in Fig. 2), with the general formula $NbO_y(H_2O)_w^+$ ($y = 2$, 4, 6, 8, $w = 1$, 3) were generated from water impurities present in the gas inlet system.

3.2 Fragmentation channels

Another striking feature in Fig. 2 is the intensity increase in all peaks when the secondary beam is on. Considering all the possible outcomes of cluster ion–atom collisions (Eqs. i–v), this increase can be attributed to energetic neutral fragments (Eqs. ii, iii) and/or to the creation of additional charged species by Coulomb explosion (Eq. v). This second possibility will be discussed later. The newly formed ionic species can be separated from the nonfragmented parent by gradually increasing the RFEA voltages (V_{grid}) and measuring the decrease in the signal for each particular cluster as already mentioned in Sect. 2.2.

The signal's evolution with increasing V_{grid} between 0 and $\sim$2,000 V ($V_{grid} \gg V_{acc}$) is shown in Fig. 3 for NbO_8^+. The determination of fragments' masses, as described in the Sect. 2.2, indicates that NbO_y^+ clusters dissociate via loss of one or more O_2 molecules (or pairs of oxygen atoms).

The fragmentation pathways for the NbO_y^+ clusters are also investigated with the conventional gas cell experimental configuration described in Sect. 2.2. In investigations using a reflectron [29], similar results were obtained for all NbO_y^+ clusters, and we present in Fig. 4 only the

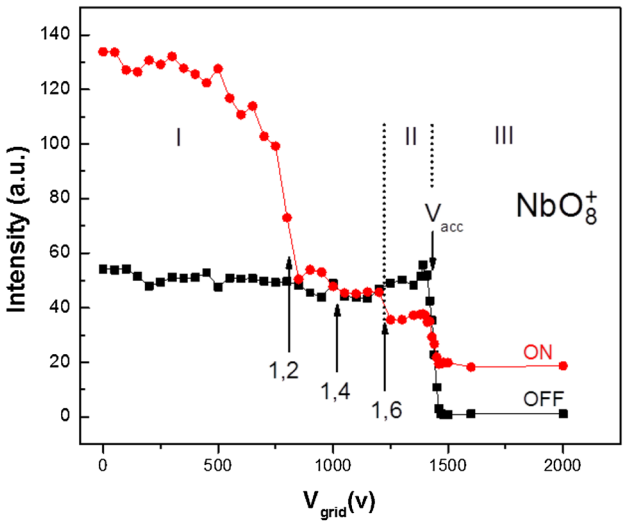

Fig. 3 The fragmentation of the NbO_8^+ clusters. The *arrows* with the labels indicate the kinetic energy and the size of the corresponding fragments

case of NbO_8^+ as a representative example (collision partner Kr, collision energy in the center of mass frame, $E_{CM} = 275$ eV).

Both methods clearly indicate similar fragmentation patterns, showing the loss of one or more O_2 molecules. The mass of the neutrals cannot be directly measured, but is calculated as the difference between the masses of the parent and the observed ionic fragments; therefore, the form of oxygen fragments (atomic or molecular) is undetermined. Loss of two O atoms or, more likely, molecular oxygen it is one of the fragmentation channels of larger Nb_xO_y clusters for highly energetic collisions [13] and the main photofragmentation channel for oxygen-rich Nb_2O_n clusters [16]. In our group, it has also been previously observed for FeO_{2y}^+ ($y \leq 6$) clusters [21, 36].

The loss of oxygen is also observed for clusters containing two Nb atoms. In Fig. 5, we present the intensity of $Nb_2O_8^+$ cluster, as a function of the V_{grid} before and after secondary beam crossing, and we indicate in figure by arrows and labels the kinetic energy and the size *x,y* of the expected fragments, respectively.

3.3 Collision cross section measurements

As analyzed before in Sect. 2.2, the fragmentation cross section Q for an individual cluster is determined using Eq. (4). In particular, for the $Nb_xO_y^+$ clusters in collisions with Ne atoms with an acceleration potential of 1,500 V we use:

$$Q = -\frac{1}{NL}\ln\left(\frac{I^{ON}_{Vgrid=1400} - I^{ON}_{Vgrid=2000}}{I^{OFF}_{Vgrid=1400} - I^{OFF}_{Vgrid=2000}}\right). \quad (4)$$

In Fig. 6, we plot the *QNL* values obtained from the crossed beam (CB) fragmentation of NbO_y^+ clusters as a function of the number of oxygen atoms *y*, for three values of the laboratory collision energy (500, 1,500, and 1,800 eV). For comparison, Fig. 6 also shows the *QNL* results (circles) obtained using the conventional beam-gas cell (BG) configuration, at $E_{Lab} = 1{,}500$ eV. The data sets were normalized to each other using the least square method. Some representative error bars (~20 %) (due mainly to the reproducibility of the data) are also shown in figure. The CB and BG results are in good agreement, showing a similar trend of increasing cross section with increasing *y* for NbO_y^+ ($y = 4, 6, 8$) clusters, as predicted by the quasi-spherical cluster model [41]. As notable exception, for NbO_{10}^+ the fragmentation cross section is equal or smaller than for NbO_8^+. A similar situation was observed for iron oxide clusters [21, 36], and it was explained by an increased stability of FeO_{10}^+, as proved by the corresponding mass spectra and the DFT calculations. In the same way, in the present case, the mass spectrum of niobium oxide clusters supports this assumption, showing an intense peak for NbO_{10}^+, followed by an important signal decrease for the next clusters of the series.

The fragmentation cross section is the lower limit and in certain conditions represents a good approximation of the total collision cross section [21]. Under these circumstances, the evolution of the fragmentation cross section as a function of cluster size should be independent of the collision energy. In order to prove this, cross section measurements of NbO_y^+ clusters were performed for three different values of kinetic energy in the laboratory frame of reference E_{Lab} at 500, 1,500, and 1,800 eV. The results are very similar and can be explained by the fact that even at the lowest E_{Lab} investigated here (500 eV), the collision energy is high enough (E_{CM} ranges from 37 eV for NbO_{10}^+ to 70 eV in the case of NbO_2^+) and every collision leads to cluster fragmentation.

This is also the case for the beam-gas cell experiments, performed with Kr as a collision partner. The larger mass of Kr ($m = 84$), as compared to Ne ($m = 20$), makes that for similar laboratory energies, the center of mass collision energy is higher. Moreover, increasing the E_{CM} by increasing the accelerating potential to 1,800 V (up to 248 eV for NbO_2 in collision with Ne) did not lead to the appearance of new (high energy activated) fragmentation channels.

In our previous work on iron oxide clusters [21, 36], the equivalence between the fragmentation cross section and the total collision cross section at high collision energies has been proved by comparing the experimental results with the calculated geometrical cross sections for theoretical structures. To the best of our knowledge, such

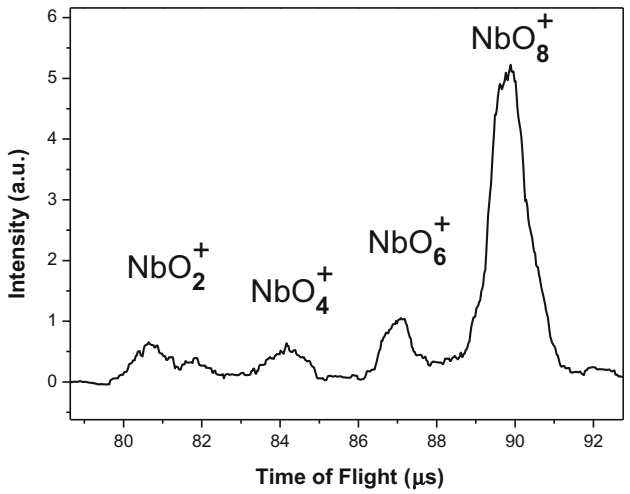

Fig. 4 Reflectron TOF spectrum of the mass-selected NbO_8^+ cluster, showing the fragments formed after collisions with Kr atoms in beam-gas cell arrangement

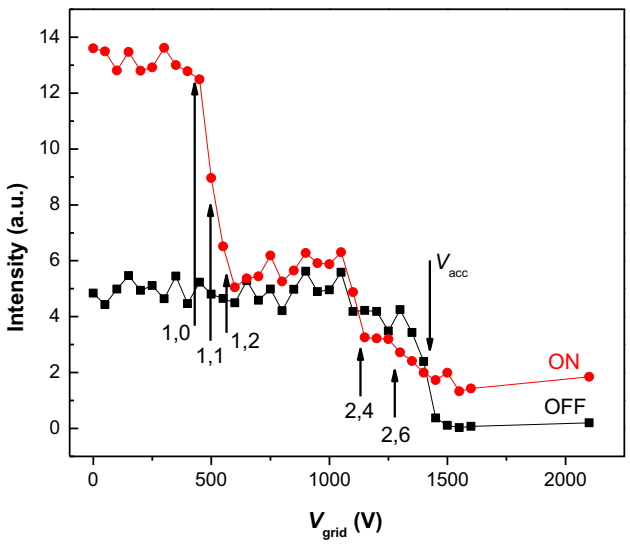

Fig. 5 The fragmentation of the $Nb_2O_8^+$ cluster

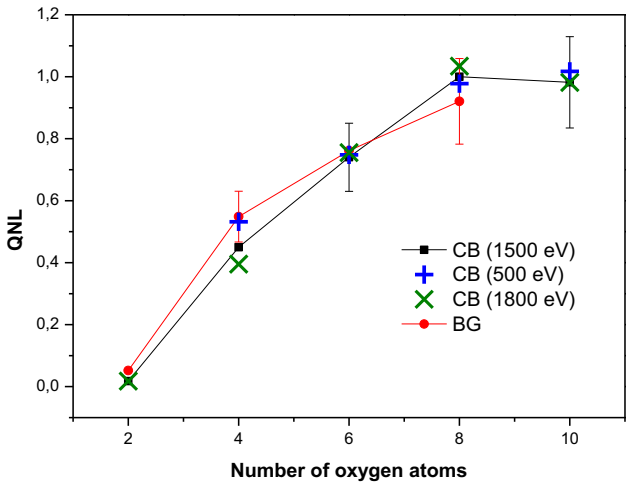

Fig. 6 Fragmentation cross sections of NbO_y^+ clusters. The values were obtained from the crossed beam (CB) experiments with secondary Ne beam at different laboratory collision energies (*square* 1,500 eV, *cross* 1,800 eV, and *plus* 500 eV) and the beam-gas cell (BG) experiments using Kr as the collision gas (*circle*) at 1,500 eV collision energy

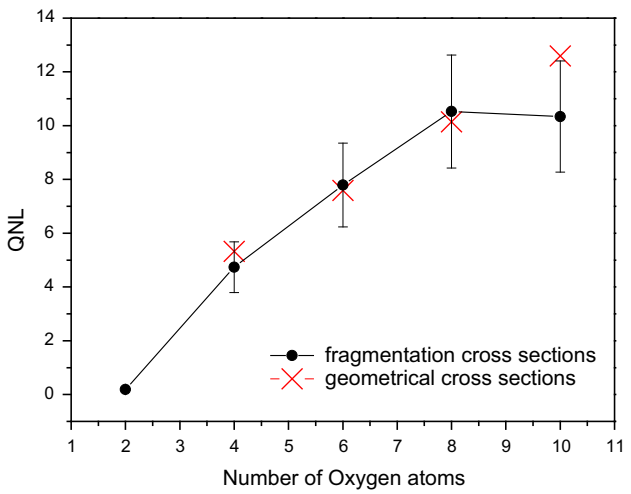

Fig. 7 Comparison of experimentally determined fragmentation cross sections (CB experiments at collision energy 1,500 eV) and calculated geometrical cross section for NbO_y^+ clusters

structures are not available for the (quite uncommon) oxygen-rich clusters containing one niobium atom (ion) reported here. We noticed, however, some similarities between the experimental results (compare mass spectra and QNL measurements from this paper with Refs. [21, 36]) obtained for niobium and iron oxides clusters, like the prevalence of clusters containing an even number of oxygen atoms and the stability of clusters with 10 oxygen atoms followed by a sudden decrease in the intensity for larger clusters. Similar evolution is noticed also in the case of the fragmentation cross sections of the two series: a linear increase with the size, with the small decrease for MO_{10} clusters (M = Nb or Fe). These similarities encouraged us to assume similar geometries for niobium oxide and iron oxide clusters. In addition, we approximated the length of different bonds between the constituent atoms from structures reported in the literature for larger niobium oxide clusters (containing more than 1 Nb atom) [14, 43, 44]. We considered the distance between Nb and O to be 1.9 and 1.75 Å, for a single bond and double bond, respectively, and the length of O–O bond to be 1.3 Å. By rescaling the iron oxide clusters structures reported in Ref. [42] to the bond lengths mentioned earlier, we determined some probable geometries for the NbO_n^+ clusters studied here.

In Fig. 7, we compare the fragmentation cross section measured in the crossed beam experimental configuration and the geometrical cross sections determined by applying the projection model to structures considered as most probable for O-rich NbO_n^+ clusters. As in the case of iron oxide clusters, a good correspondence is observed between most of the experimental and theoretical values. The only discrepancy, observed for NbO_{10}^+, can be explained (like for FeO_{10}^+) by the fact that in theory, we calculate the geometrical cross section, which is only approximated with the fragmentation cross section determined experimentally. This effect is evident also for the thermodynamically stable NbO_2^+: its fragmentation cross section as measured by our method is very small, close to zero in the error limits.

Cross section determination using the crossed beam configuration does not require prior mass separation of individual clusters. In this way, even clusters with a low abundance can be measured. As already mentioned, in our source, clusters with more than one metal atom are scarcely formed (see Fig. 2), but their intensity is enough to allow cross beam measurements. In Fig. 8, we plot the results (squares) for the fragmentation cross section of $Nb_2O_y^+$ clusters as a function of the number of the oxygen atoms y at $E_{lab} = 1{,}500$ eV.

As expected, the general trend of the increasing cross section with the cluster size is observed. Furthermore, it is worth noticing that the fragmentation cross sections reflect also the stability of the clusters, so that the local minima in the cross section indicate higher stability of the respective clusters. This is in accordance with the mass spectra of Fig. 2, where the stability of the same clusters appears as peaks with higher intensity. As previously observed for NbO_{10}^+, in this case $Nb_2O_6^+$, $Nb_2O_8^+$, and $Nb_2O_{10}^+$ seem to be more stable in comparison with their neighbors.

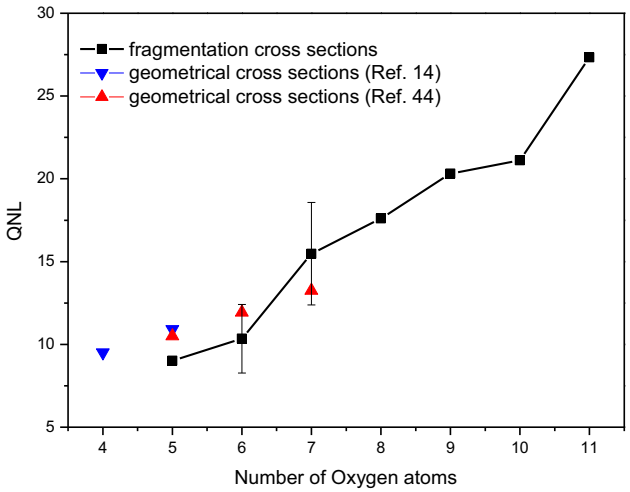

Fig. 8 $Nb_2O_y^+$ clusters fragmentation cross sections obtained from the crossed beam experiments at $E_{Lab} = 1{,}500$ eV and the calculated geometrical cross section for structures from Refs. [14, 44]

Several authors [14, 43, 44] reported calculations of low energy structures for Nb_2O_n clusters (neutrals and/or ions). For the Nb_2O_4 and Nb_2O_5 [14], the differences between the neutral and cationic structures are insignificant; they have the same geometries; only the bond lengths are slightly different. This allows us to use the neutral geometries reported by Zhai et al. [44] as an approximation for larger clusters' structures, and we used the projection model to determine their geometrical cross section. The calculated values (triangles) agree with the experimentally determined fragmentation cross sections in the limit of the experimental errors. Theoretical calculations are necessary for larger clusters in order to have a more thorough comparison.

3.4 Collisional multi-ionization

If the outcome from a collision between a cluster ion (AB^+) and an atom (X) is the fragmentation

$$AB^+ + X \rightarrow A^+ + B + X,$$

then the intensity of parents (AB^+) and the ionic fragments (A^+) varies with V_{grid} as presented in Fig. 1. In the case of NbO_y^+ clusters, B would correspond to an undetermined number of neutral oxygen molecules or atoms produced by fragmentation. It is assumed that for $V_{grid} \approx 0$, the intensity difference between "beam on" and "beam off" is exclusively due to the neutral fragments (B). The amount of these neutrals can be measured when $V_{grid} \gg V_{acc}$ with the secondary beam "on" (the charged species are rejected and only neutrals are detected).

However, this is not the case for the experimental data shown in Fig. 3, where the high intensity of clusters at $V_{grid} \approx 0$ after the interaction with the secondary beam exceeds the amount of the neutrals and thus clearly indicates the appearance of new ions. Additional charges can be formed from one ion by Coulomb explosion of a multiply charged cluster, as indicated in Eq. (5).

$$AB^+ \xrightarrow{+Ne} AB^{z+} + (z - 1)e^- \longrightarrow AB^{x+} + B^{(z-x)+} + (z - 1)e^- \quad (5)$$

The first ionization potentials of both molecular ($IP(O_2) = 12.07$ eV) and atomic ($IP(O\ I) = 13.6$ eV) oxygen [45] are smaller than the second ionization potential of niobium ($IP(Nb\ II) = 14.32$ eV) [46], so no stable $Nb^{2+}O_y$ clusters are expected to be formed. Instead, the second charge will appear on one of the O atoms and because the cluster is not big enough to compensate the Coulombic repulsion by charge separation, a positively charged fragment will be ejected. It is well known that multiply charged clusters are observed only above a critical size (appearance size); for example, pure Nb_n^{2+} clusters

Table 1 Ratio of ions detected after collisions to the initial parent ions at different acceleration energies

Cluster ion	$V_{acc} = 500$ V	$V_{acc} = 1{,}500$ V	$V_{acc} = 1{,}800$ V
NbO_4^+	1.14	1.36	1.94
NbO_6^+	1.25	1.82	2.20
NbO_8^+	1.31	2.21	2.42
NbO_{10}^+	1.35	2.52	2.50

have been detected only for $n \geq 9$. [46] For a discussion on charge delocalization dynamics on metal clusters and metal oxide clusters, see Refs. [47, 48].

The ratio of charged particles formed following collisional activation to the initial parents is noted $(I_0 + CE)/I_0$ and can be determined from the cluster's intensity measured at $V_{grid} \approx 0$, where all the fragments are detected (region I in Fig. 3) using the formula:

$$\frac{I_0 + CE}{I_0} = \frac{I_{\mathrm{I}}^{\mathrm{ON}} - I_{\mathrm{III}}^{\mathrm{ON}}}{I_{\mathrm{I}}^{\mathrm{OFF}} - I_{\mathrm{III}}^{\mathrm{OFF}}}, \quad (6)$$

where I_0 is the intensity of the parent and CE represents additional ions formed by Coulomb explosion. $I_{\mathrm{I}}^{\mathrm{ON}}$, $I_{\mathrm{III}}^{\mathrm{ON}}$, $I_{\mathrm{I}}^{\mathrm{OFF}}$ and $I_{\mathrm{III}}^{\mathrm{OFF}}$ are the intensities measured in regions I and III for "beam on" and "beam off," respectively. In Table 1, we present the values obtained for NbO_y^+ clusters at three different acceleration energies.

Values of the ratio superior to 1 prove the formation of new charges by Coulomb explosion in all studied cases, for example, 14 % of supplementary charges formed from NbO_4^+. The ratio superior to 2 indicates at least one channel leading to the appearance of two or more new charges. For the clusters considered, the fraction of newly formed ions to the initial parents is increasing with the cluster size, indicating the loss of more ionic fragments from larger clusters.

For any particular cluster, the increase in acceleration energy promotes the formation of more charged fragments. This can be explained by the fact that at higher collision energy, more energy is transferred to the cluster electronic excitations, possibly removing many electrons and resulting in the formation of higher z multiply charged ions that will produce more fragment ions. A thorough study of the extent of Coulomb explosion for various (high) collision energies, feasible using our technique, would give information on the parent cluster's energetic states and multiionization phenomena.

4 Conclusions

In this paper, we present the formation and fragmentation of $Nb_xO_y^+$ clusters ($x = 1, 2$, $y = 2$–12) after collision with noble gases. The open configuration of our cluster source, combined with the use of a high oxygen content beam for the clusters formation, leads to the apparition of small, oxygen-rich aggregates whose O/Nb ratio is very different from the stoichiometry of the common niobium oxides.

We also measured the collision cross sections of those clusters. The results are based on the fragmentation cross sections, obtained following collision-induced dissociation.

Without precisely measuring the N (the number density of the collision partner) and L (the length of the interaction region between clusters and noble gas), the absolute value cannot be determined, but the evolution of measured cross section with the cluster's size (number of atoms) is representative and could be used for validating structures obtained by ab initio calculations, as we have recently shown. [21]

While the conventional CID studies using a reflectron are limited (by ion optics) to the detection of fragments with molecular masses close to the parents', the linear configuration used in our new approach allows the efficient detection of ions (and neutrals!) in a larger mass range. Therefore, the new experimental configuration allows detecting and quantifying the Coulomb explosion of small clusters, opening the way to new studies.

Acknowledgments C.M. acknowledges support by the Romanian National Authority for Scientific Research, CNCS—UEFISCDI, project number PN-II-RU-TE-2011-3-0174. P.G. acknowledges financial support by Marie Curie Initial Training network ICONIC (Grant No. PITN-GA-2009-238671).

References

1. I.E. Wachs, L.E. Briand, J.-M. Jehng, L. Burcham, X. Gao, Catal. Today **57**, 323 (2000)
2. E.I. Ko, J.M. Hupp, F.H. Rogan, N.J. Wagner, J. Catal. **84**, 85 (1983)
3. T. Ushikubo, Catal. Today **57**, 331 (2000)
4. J.-M. Jehng, I.E. Wachs, Catal. Today **8**, 37 (1990)
5. S. Yoshida, Y. Nishimura, T. Tanaka, H. Kanai, T. Funabiki, Catal. Today **8**, 67 (1990)
6. A. Morikawa, A. Togashi, Catal. Today **16**, 333 (1993)
7. Y. Zhao, X. Zhou, L. Ye, S.C.E. Tsang, Nano Rev. **3**, 17631 (2012)
8. A. Borgschulte, J.H. Rector, B. Dam, R. Griessen, A. Züttel, J. Catal **235**, 353 (2005)
9. S.W. Sigsworth, A.W. Castleman Jr, J. Am. Chem. Soc. **114**, 10471 (1992)
10. M.R. Sievers, P.B. Armentrout, Int. J. Mass Spectrom. **179–180**, 103 (1998)
11. P. Jackson, K.J. Fisher, G.D. Willett, Int. J. Mass Spectrom. **197**, 95 (2000)
12. P. Jackson, K.J. Fisher, G.D. Willett, Chem. Phys. **262**, 179 (2000)
13. H.T. Deng, K.P. Kerns, A.W. Castleman Jr, J. Phys. Chem. **100**, 13386 (1996)
14. J.R. Sambrano, J. Andrés, A. Beltrán, F. Sensato, E. Longo, Chem. Phys. Lett. **287**, 620 (1998)

15. A. Fielicke, G. Meijer, G. von Helden, J. Am. Chem. Soc. **125**, 3659 (2003)
16. K.S. Molek, T.D. Jaeger, M.A. Duncan, J. Chem. Phys. **123**, 144313/1 (2005)
17. G.S. Fanourgakis, S.C. Farantos, C. Lüder, M. Velegrakis, S.S. Xantheas, J. Chem. Phys. **109**, 108 (1998)
18. M. Velegrakis, A. Sfounis, Appl. Phys. A **97**, 765 (2009)
19. M. Jadraque, B. Sierra, A. Sfounis, M. Velegrakis, Appl. Phys. B **100**, 587 (2010)
20. M. Velegrakis, M. Massaouti, M. Jadraque, Appl. Phys. A **108**, 127 (2012)
21. M. Velegrakis, C. Mihesan, M. Jadraque, J. Phys. Chem. A **117**, 2891 (2013)
22. W. Begemann, S. Dreihöfer, K.H. Meiwes-Broer, H.O. Lutz, Z. Phys. **3**, 183 (1986)
23. G. von Helden, M.T. Hsu, N. Gotts, M.T. Bowers, J. Phys. Chem. **97**, 8182 (1993)
24. M.F. Jarrold, J. Phys. Chem. **99**, 11 (1995)
25. C. Lüder, M. Velegrakis, J. Chem. Phys. **105**, 2167 (1996)
26. C. Lüder, E. Georgiou, M. Velegrakis, Int. J. Mass Spectrom. Ion Processes **153**, 129 (1996)
27. G.E. Froudakis, M. Muhlhauser, S.C. Faranto, A. Sfounis, M. Velegrakis, Chem. Phys. **280**, 43 (2002)
28. E. Witkowicz, H. Linnartz, C.A. de Lange, W. Ubachs, A. Sfounis, M. Massaouti, M. Velegrakis, Int. J. Mass Spectrom. **232**, 25 (2004)
29. J.R. Stairs, T.E. Dermota, E.S. Wisniewski, A.W. Castleman Jr, Int. J. Mass Spectrom. **213**(1), 81 (2002)
30. M. Barat, J.C. Brenot, J.A. Fayeton, Y.J. Picard, Rev. Sci. Instrum. **71**, 2050 (2000)
31. K. Athanassenas, D. Kreisle, B.A. Collings, D.M. Rayner, P.A. Hackett, Chem. Phys. Lett. **213**, 105 (1993)
32. P.P. Radi, G. von Helden, M.T. Hsu, P.R. Kemper, M.T. Bowers, Int. J. Mass Spectrom. Ion Processes **109**, 49 (1991)
33. F. Dong, S. Heinbuch, S.G. He, Y. Xie, J.J. Rocca, E.R. Bernstein, J. Chem. Phys. **125**, 164318 (2006)
34. S.K. Loh, Li Lian, P. B. Armentrout. J. Chem. Phys. **91**, 6148 (1989)
35. M. Chen, X. Wang, Q. Qin, Appl. Surf. Sci. **156**, 16 (2000)
36. G. Mpourmpakis, M. Velegrakis, C. Mihesan, A.N. Andriotis, J. Phys. Chem. A **115**, 7456 (2011)
37. K.A. Zemski, D.R. Justes, A.W. Castleman Jr, J. Phys. Chem. B **106**, 6136 (2002)
38. D. Prekas, C. Lüder, M. Velegrakis, J. Chem. Phys. **108**, 4450 (1998)
39. M. Velegrakis, *Advances in metal and semiconductor clusters*, chap. 7, vol. *V*, ed. by M.A. Duncan (Elsevier, Amsterdam, 2001), pp. 227–265
40. C. Lüder, D. Prekas, M. Velegrakis, Laser Chem. **17**, 109 (1997)
41. P. Weis, Int. J. Mass Spectrom. **245**, 1 (2005)
42. C. Wang, J. Jian, G. Wang, Z.H. Li, M. Zhou, J. Phys. Chem. A **118**, 4519 (2014)
43. Y.X. Zhao, X.L. Ding, Y.P. Ma, Z.C. Wang, S.G. He, Theor. Chem. Acc. **127**, 449 (2010)
44. H.J. Zhai, X.H. Zhang, W.J. Chen, X. Huang, L.S. Wang, J. Am. Chem. Soc. **133**, 3085 (2011)
45. H.M. Rosenstock, K. Draxl, B.W. Steiner, J.T. Herron, *"Ion Energetics Data" in NIST Chemistry WebBook, NIST Standard Reference Database Number 69*, Eds. by P.J. Linstrom, W.G. Mallard, National Institute of Standards and Technology, Gaithersburg MD, 20899, http://webbook.nist.gov, (retrieved 18 Sept 2013)
46. N. Saito, K. Koyama, M. Tanimoto, Appl. Surf. Sci. **169–170**, 379 (2001)
47. T. Döppner, S. Teuber, M. Schumacher, J. Tiggesbäumker, K.H. Meiwes-Broer, Appl. Phys. B **71**, 357 (2000)
48. D.E. Blumling, S.G. Sayres, A.W. Castleman Jr, Int. J. Mass Spectrom. **300**, 74 (2011)